MEMS-based Material Testing Systems

1.   Introduction

In the early 1990s, Iijima (1991) discovered a one-dimensional (1D) nanostructure, the carbon nanotube (CNT), which sparked an entirely new avenue within nanoscience and nanotechnology. Nanowires (NWs) (Cui and Lieber 2001), nanorods (Li and Alivisatos 2003), nanotubes (Wang and Li 2003), and nanobelts (Pan et al. 2001) of various materials have been successfully synthesized shortly afterwards. These 1D nanostructures demonstrate novel mechanical (Yu et al. 2000), electronic (Wildoer et al. 1998),

and optical properties (Duan et al. 2003). Potential applications for these structures range from nano-electromechanical systems (NEMSs) (Fennimore et al. 2003) to nanoelectronics (Cui et al. 2001) to nanophotonics (Law et al. 2004).

A large number of NEMS devices based on nanostructures have been realized. Fennimore et al. (2003) reported a CNT-based rotational motor (Fig. 1(a)). Kim and Lieber (1999) reported CNT-based nanotweezers (Fig. 1(b)). Multiwalled carbon nanotubes (MWCNTs) actuated by electrostatic force were used as the tweezers' arms.

NTs and NWs have been demonstrated as building blocks in logic circuits (Bachtold et al. 2001, Huang et al. 2001). In addition, they have been used as highly
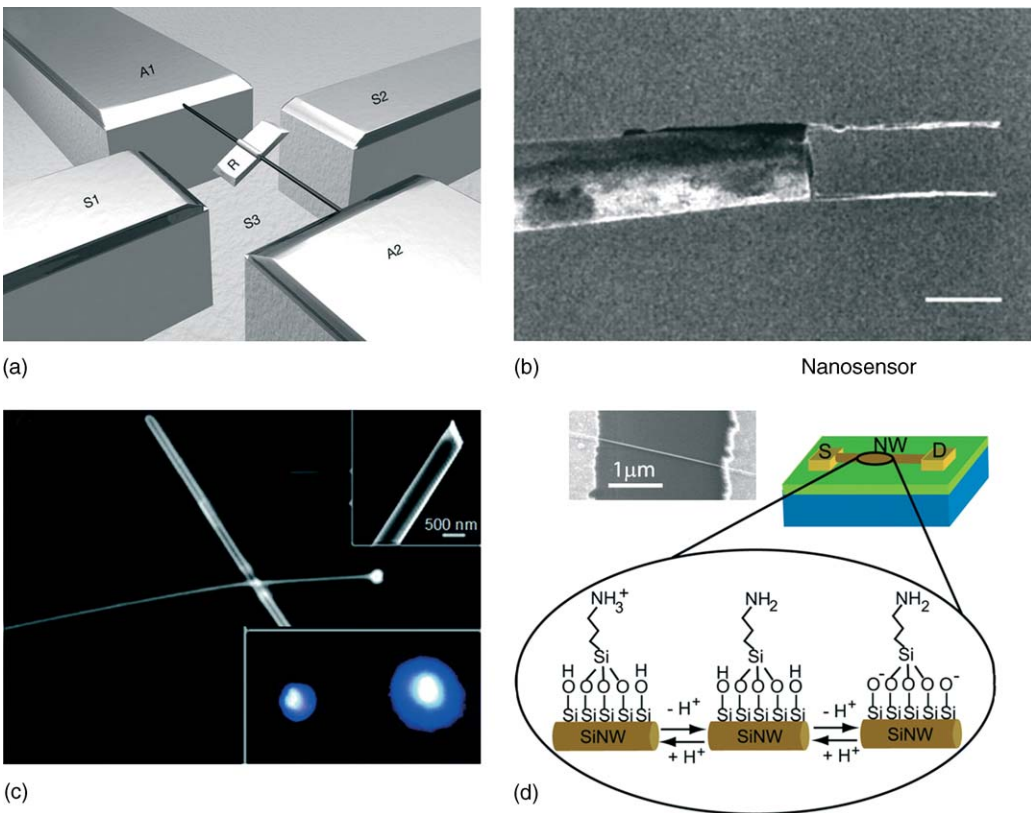

Figure 1
(a) Schematic of the nanotube-based NEMS motor. Reproduced by permission of Nature Publishing Group from *Nature*, **424**, 2003, 408. (b) Nanotube-based nanotweezers. Scale bar, 2 μm. Reproduced by permission of American Association for the Advancement of Science from *Science*, 2000, **286**, 2148. (c) Dark field photoluminescence view of a nanoribbon at the right end, with the laser focused on the left end. A wide (~1 μm) ribbon lies across the ribbon of interest, (inset, bottom). The guided emission during nonresonant excitation with monochromatic blue light. The left emission spot is caused by scattering at the ribbon–ribbon junction and the right spot is at the right end of the nanoribbon. Reproduced by permission of American Association for the Advancement of Science from *Science*, 2004, **305**, 1269. (d) An NW nanosensor for pH detection. Zoom of the surface modified SiNW illustrating changes in the surface charge state with pH. (inset) SEM image of a typical SiNW nanosensor. Reproduced by permission of American Association for the Advancement of Science from *Science*, 2001, **293**, 1289.

sensitive and selective sensors for detecting gas, chemical, and biological species. Gas sensors based on individual single-walled CNTs (SWCNTs) were demonstrated (Kong *et al.* 2000). Upon exposure to gaseous molecules such as NO_2 or NH_3, the electrical resistance of a semiconducting SWCNT is found to dramatically increase or decrease. Nanosensors based on boron-doped silicon nanowires (SiNWs) were used to detect a variety of chemical and biological species (Cui *et al.* 2001) (Fig. 1(d)). For instance, antigen-functionalized SiNWs showed reversible antibody binding and concentration-dependent detection.

In addition to nanoelectronics and nanostructures, CNTs are finding their ways in nanophotonics. A large number of applications in photonics have been demonstrated including waveguides, light-emitting diodes, lasers, and photodetectors. An important issue in developing nanophotonics is to achieve a nanostructure waveguide that can link these various elements. As a first step, assembly of nanoribbon waveguides with nanowire light sources and detectors has been demonstrated recently (Law *et al.* 2004) (Fig. 1(c)).

To fully utilize the basic and technological advantages offered by the nanostructures, there are three key challenges to be overcome for the future technological applications. First, synthesis of size, morphology, and structure controlled nanostructures, and thus possible control of their properties; second, characterization of the properties of individual nanostructures; and finally, integration of nanostructures with the existing technology for broad applications, especially in nanoscale electronics and optoelectronics. It is the purpose of this article to address the second aspect by reviewing the mechanical characterization of nanostructures by means of on-chip testing techniques. Likewise, a novel material testing system based on microelectromechanical systems (MEMSs) for nanostructures will be described with applications.

2. Mechanical Testing of 1D Nanostructures

Characterizing the mechanical properties of individual 1D nanostructures is a grand challenge not easily met by many existing testing and measuring techniques because of the following requirements: (i) constructing appropriate tools to manipulate and position specimens, (ii) applying and precisely measuring forces in the nano-newton range, and (iii) measuring local mechanical deformation precisely. To date, the experimental techniques employed in the mechanical testing of 1D nanostructures can be roughly grouped into three major categories: dynamic vibration, bending, and tensile testing.

2.1 Dynamic Vibration

Treacy *et al.* (1996) estimated the Young's modulus of MWCNTs by measuring the amplitude of their thermal vibrations during *in situ* transmission electron microscope (TEM) imaging. The nanotubes were attached to the edge of a hole in 3-mm-diameter nickel rings for TEM observation, with one end clamped and the other free. The TEM images were blurred at the free ends, and the blurring was significantly increased with the temperature increase of the NTs. This indicated that the vibration was of thermal origin. Blurring occurs because the vibration cycle is much shorter than the integration time needed for capturing the TEM image. The Young's modulus was estimated from the envelope of the thermal vibration.

Poncharal *et al.* (1999) measured the Young's modulus of MWCNTs using a method based on mechanical resonance. The actuation was achieved utilizing an AC electrostatic field within a TEM (Fig. 2(a)). In the experiment, the nanotubes were attached to a fine gold wire, on which a potential was applied. In order to precisely position the wire near the grounded electrode, a special TEM holder with a piezo-driven translation stage and a micrometer-resolution translation stage was used. Application of an AC voltage to the nanotubes caused a time-dependent deflection. The elastic modulus was then estimated from the observed resonance frequencies.

2.2 Bending Test

Wong *et al.* (1997) measured Young's modulus, strength and toughness of MWCNTs, and SiC NRs using an atomic force microscope (AFM) in the lateral force mode (Fig. 2(b)). In their method, the nanostructures were dispersed randomly on a flat surface and pinned to the substrate by means of microfabricated patches. Then AFM was used to bend the cantilevered nanostructures transversely. At a certain location along the length of each structure, the force versus deflection (*F–d*) curve was recorded to obtain the spring constant of the system. Multiple *F–d* curves were recorded at various locations along the structure. By considering the nanostructure as a beam, the *F–d* data were used to estimate Young's modulus.

Bending of nanostructures resting on a substrate is straightforward to implement. Nevertheless, it cannot eliminate the effect of adhesion and friction from the substrate. To solve the friction issue, Walters *et al.* (1999) suspended the nanotube over a microfabricated trench and bended the nanotube using AFM in the lateral force mode. Salvetat *et al.* (1999) introduced a similar method by dispersing MWCNTs on alumina ultrafiltration membrane with 200 nm pores. The adhesion between the nanotubes and the membrane was found to be sufficiently strong to fix the two ends. Using AFM in the contact mode, the authors deflected the suspended NTs vertically.
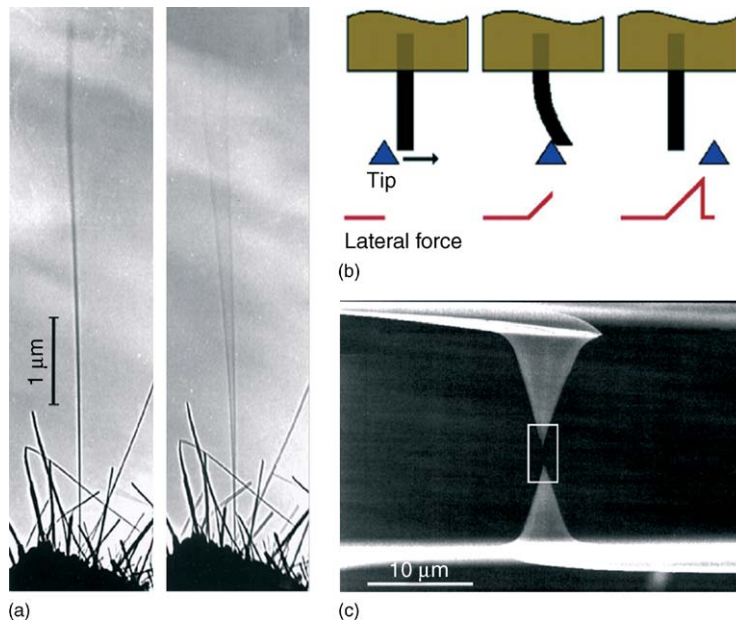
Figure 2
(a) Dynamic responses of an individual CNT to alternate applied potentials, (left) absence of a potential, and (right) at fundamental mode. Reproduced by permission of American Association for the Advancement of Science from *Science*, 1999, **283**, 1513. (b) A CNT with one end clamped is deflected by an AFM in the lateral force mode. Reproduced by permission of American Association for the Advancement of Science from *Science*, 1997, **277**, 1971. (c) An individual MWCNT mounted between two opposing AFM tips and stretched uniaxially by moving one tip. Reproduced by permission of American Association for the Advancement of Science from *Science*, 2000, **287**, 637.

2.3 Tensile Test

Pan *et al.* (1999) used a stress–strain rig to pull a very long (~2 mm) MWCNT rope containing tens of thousands of parallel tubes. Yu *et al.* (2000) conducted an *in situ* SEM tensile testing of MWCNTs with the aid of a nanomanipulator (Fig. 2(c)). A single nanotube was clamped to the AFM tips by localized electron beam induced deposition (EBID) of carbonaceous material inside the SEM chamber. The experimental setup consisted of three parts: a soft AFM probe (force constant less than $0.1 \, N \, m^{-1}$) as a load sensor, a rigid AFM probe as an actuator, which was driven by a linear motor, and the nanotubes mounted between two AFM tips. Following the motion of the rigid cantilever, the soft cantilever was bent due to the tensile load, equal to the force applied on the nanotube. The nanotube deformation was recorded by SEM imaging, and the force was measured by recording the deflection of the soft cantilever. The Young's modulus and the failure strength of MWCNTs were measured using this method.

Although significant progress has been achieved, the mechanical testing of nanostructures is still quite rudimental. This is in large part due to the lack of control in experimental conditions and the lack of accuracy in force and displacement measurements. Recent advances in MEMSs offer a promising class of actuators and sensors, which can be advantageously employed in the testing of micro- and nanoscale specimens.

3. MEMS On-chip Testing

MEMSs consist of micromachined elements, such as comb-drive actuators and strain sensors that can be integrated on a chip. They have the potential to impact the small-scale testing field through high-resolution force and displacement measurements. Actually, MEMSs have been used successfully in the mechanical testing of MEMS materials.

An MEMS-based testing approach employs a comb-drive actuator to achieve time-dependent stressing of the specimen through voltage modulation (e.g., van Arsdell and Brown 1999). The device architecture consists of the microscale specimen with one end attached to a rigid mount and the other to a large perforated plate, which sweeps in an arc-like fashion when driven electrostatically by a comb-drive actuator (Fig. 3(b)). The resulting motion of the structure is recorded capacitively by the comb-drive
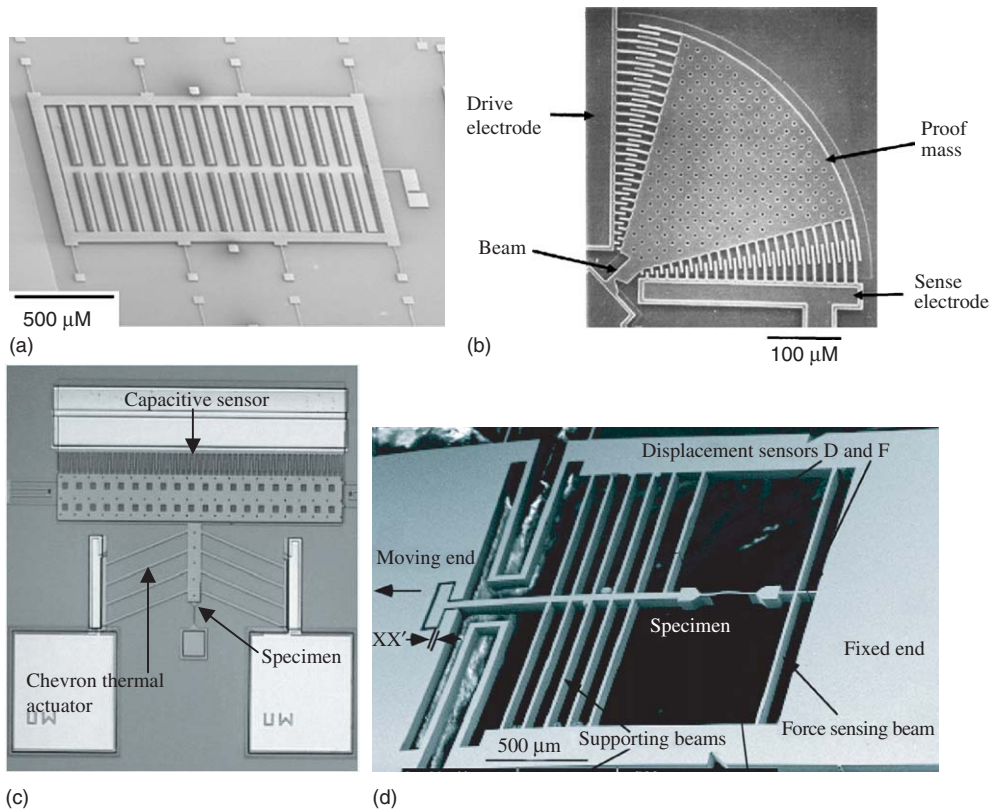
Figure 3
(a) A comb-drive actuator used in the fracture toughness test. Reprinted from *Sensors and Actuators* A, **82**, Kahn H *et al*., Fracture toughness of polysilicon MEMS devices, 274–280, copyright 2000, with permission from Elsevier. (b) An arc-like comb-drive actuator used in the fatigue test. Reprinted from van Arsdell W W, Brown S B *J. Microelectromech. Syst.* **8**, 319 (1999) © 1999, Institute of Electrical and Electronics Engineers. (c) A thermal actuator and a capacitive sensor used in tensile test. Reproduced from Fischer E E, Labossiere P E 2002 MEMS fatigue testing to study nanoscale material response. *Proc. of the SEM Ann. Conf. on Exp. and Appl. Mech.*, Milwaukee, WI, USA, with permission from Society for Experimental Mechanics, Inc. (d) An MEMS chip for the tensile test including a freestanding thin film and a force sensor. It is actuated by an external piezoelectric actuator. Reproduced from Haque M A, Saif M T A (2004) Deformation mechanisms in free-standing nanoscale thin films: a quantitative *in situ* transmission electron microscope study. *Proc. Natl. Acad. Sci (USA)* **101**, 6335–40. Copyright (2004) National Academy of Sciences, USA.

sensor on the opposite side. The specimen is tested until failure. Fracture and fatigue information about the material can then be obtained.

Comb drives were also employed to measure the fracture toughness through controlled crack propagation (Kahn *et al.* 2000, 2001). The testing rig consists of a specimen anchored to a rigid support at one end and linked perpendicularly to a comb-drive actuator. The other end is attached to a beam that connects to a comb-drive actuator (Fig. 3(a)). A notch is either micromachined into the specimen (blunt notch) or a crack is propagated into the specimen through a microindent made in close proximity

to the specimen. This step is performed as an intermediate step during the microfabrication of the specimen. Upon actuation of the comb drive, the connecting beam applies loading at the specimen notch or sharp crack. At a critical value of displacement, controlled fracture is attained.

Besides comb-drive actuation, electrothermal actuation has been used in on-chip testing (Chu *et al.* 2002, Fischer and Labossiere 2002). One such device is designed such that slanted beams impose a deformation on the sample (Fig. 3(c)). By exploiting the Joule effect, local heating and expansion of the beams is achieved. The thermal actuator pulls directly on the

specimen, stressing it in uniform tension. Strain is determined from an integrated capacitive sensor and verified through digital image correlation.

A microfabricated Si single-crystal testing rig has been developed by Haque and Saif (2002, 2004). A single-crystal micromachined structure is used for stressing submicron thin films. *In situ* SEM or TEM can be performed using this structure (see Fig. 3(d)). One end of the structure is attached to a bulk piezoelectric actuator, whereas the other end is fixed. Folded and supporting beams are employed to uniformly transfer the load to the specimen, which is attached to a supporting fixed–fixed beam. This beam, of known spring constant, is then used as the load sensor. Two displacement elements are placed at either end of the specimen where the magnitude of displacement is imaged directly from the separation of beam elements.

These testing techniques show great promise to test ever-smaller specimens and are expected to have a great impact on the development of nanoscale devices. However, a major limitation is that both deformation and load are deduced from the microscopic imaging of the specimen and testing apparatus. The limitation arises from the fact that both specimen deformation and load sensor displacement need to be imaged. When high magnifications are employed, or in X-ray setups, these two measurements cannot be made simultaneously. In the case of electron microscopy, a shift of the beam between specimen and load sensor is required.

## 4. MEMS-based Material Testing System

Here we report an MEMS designed for the testing of nanostructures using an alternative approach, which is to measure the load electronically. This scheme leaves open the possibility of continuous observation of the specimen deformation and failure at high magnification, while independently measuring the applied load. Due to its small size, the MEMS is well suited for *in situ* testing of NWs, CNTs, and thin films inside SEM, TEM, AFM, and on X-ray synchrotron stages.

The device consists of three parts: actuator, load sensor, and a gap for placement of nanostructures, as shown in Figs. 4(a) and 4(b). Two types of actuators can be employed in the device design: comb-drive electrostatic actuator and in-plane thermal actuator. The comb-drive actuator is force controlled while the thermal actuator is displacement controlled, that is, it prescribes the displacement to the specimen upon a given supplied voltage.

For a description of the principle of the comb-drive actuator, see Tang *et al.* (1990). Here, we briefly describe the thermal actuator, which can deliver a large force (up to tens of milli-newton) and a moderate displacement (up to tens of micrometers). It consists of inclined freestanding beams connected to
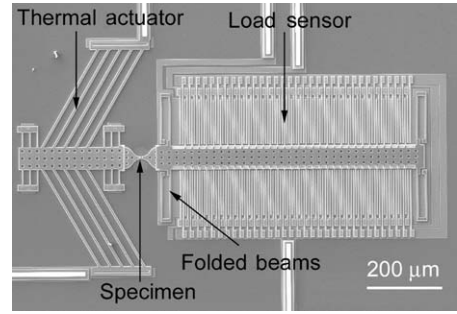
(a)
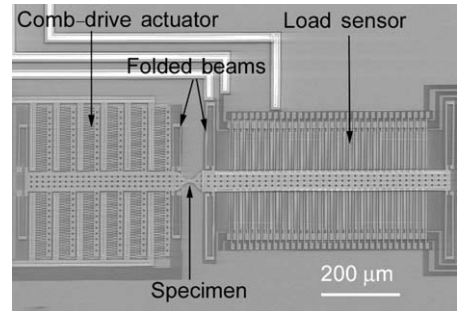
(b)

Figure 4
(a) An *in situ* tensile testing device including thermal actuator, load sensor, and specimen in between. (b) A device including comb-drive actuator, load sensor, and specimen in between. Reprinted with permission from Zhu Y, Moldovan N, Espinosa H D 2005b A microelectromechanical load sensor for *in situ* electron and X-ray microscopy tensile testing of nanostructures. *Appl. Phys. Lett.* **86**, 013506. Copyright 2005, American Institute of Physics.

a shuttle at one end and fixed to the substrate at the other end, as shown in Fig. 4(a). When a voltage is applied across the inclined beams (V-shaped beams), the current flux causes Joule-heating and thermal expansion. Due to the inclined configuration of the beams, the shuttle is pushed forward. In free motion (without connection to the specimen), the thermal actuator displacement is given as

$$U^{\Delta T} = \alpha \, \Delta T l \, \frac{\sin \theta}{\left(\sin^2 \theta + \cos^2 \theta (12I/Al^2) \right)} \qquad (1)$$

where α is the thermal expansion coefficient of the beam material, ΔT is the average temperature change in the inclined beams, l is the beam length, I is the moment of inertia of one beam in the plane parallel to the substrate $(= \frac{1}{12}Eb^3h)$, E is the Young's modulus of the actuator material, b is the beam width, h is the beam height, A is the cross-sectional area of a beam, and θ is the angle between the beams

and the transverse direction to the shuttle motion. Additional details of the design and operation of the thermal actuator can be found in Zhu and Espinosa (2005) and Zhu *et al*. (2005a).

The load sensor integrated in the testing platform is similar to the MEMS accelerometer developed by Analog Devices, Norwood, MA, in that they are both based on differential capacitive sensing and fabricated by surface micromachining. The load sensor consists of a rigid shuttle with one set of movable fingers and two sets of stationary fingers. A lumped model of the sensor consists of two capacitors in series. Shuttle displacement causes increase of one capacitance and decrease of the other. Within a moderate displacement range, the capacitance change is proportional to the displacement, namely,

$$\Delta C = C_1 - C_2 = N\varepsilon A \left(\frac{1}{d_0 - \Delta d} - \frac{1}{d_0 + \Delta d} \right)$$
$$\approx \frac{2N\varepsilon A}{d_0^2} \Delta d \tag{2}$$

where ε is the electric permittivity, N the number of units of differential capacitors, A and d_0 the overlap area and initial gap between the movable finger and each stationary finger, respectively, and Δd the displacement of the load sensor. The load sensor is anchored to the substrate by four folded beams that are designed with a range of stiffness for testing various materials of interest. For details on the load sensor principles, see Zhu *et al*. (2005b).

The devices for *in situ* testing were fabricated at MEMSCAP (Durham, NC) using the standard Poly-MUMPs process. The devices range from 1000 μm × 640 μm to 2000 μm × 1000 μm in size. A number of devices were included in one chip (10 mm × 10 mm) for the purpose of testing different materials of interest. The chip is attached to a ceramic pin grid array (PGA) package and wire bonded for electric connection. The chip is then placed in a detachable socket on a PC board (Fig. 5(a)).

In addition to the *in situ* SEM measurements here reported, this device has the potential to impact other nanoscale characterization techniques. For instance, *in situ* TEM testing of nanostructures is achievable by microfabrication of a window under the specimen area. The major challenge is to etch such a window, from the back of the silicon wafer, without damaging the previously fabricated structures. We have accomplished such task by deep reactive ion etching of the window prior to device release. Fig. 5(b) shows an MEMS chip (5 mm × 10 mm) containing four MEMS devices next to a TEM holder. The two devices in the center can be employed to perform *in situ* TEM testing, and the other two devices can be employed in calibration tests. The chip has eight contact pads for electric actuation/sensing. The chip is designed to be directly mounted on a specially designed TEM holder containing a feedthrough and interconnects to
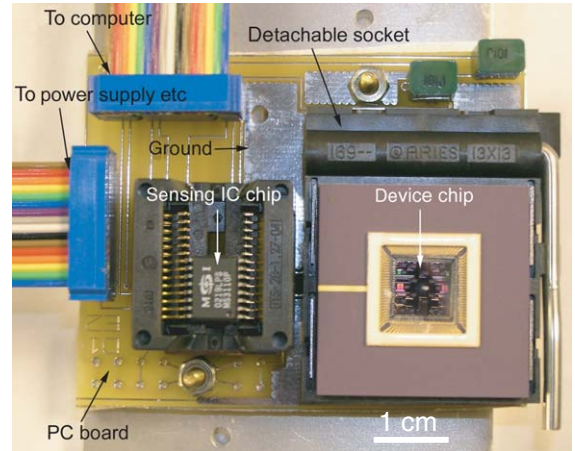
(a)
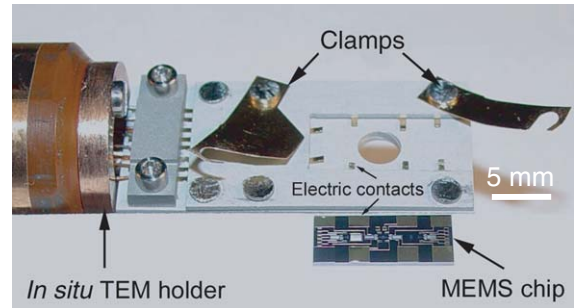
(b)

Figure 5
(a) Experimental setup for *in situ* SEM testing. MEMS device chip is positioned near the MS3110 chip on a printed circuit board. The setup is connected to a power supply, a digital multimeter, and a computer outside the SEM by means of a chamber feedthrough. (b) *In situ* TEM holder (containing a feedthrough and eight electric contact pads) along with a 5 mm × 10 mm MEMS chip. In an actual experiment, the MEMS chip is flipped, placed in the TEM holder, and fixed by the left and right clamps. Reproduced from Zhu Y, Espinosa H D (2005) An electromechanical material testing system for *in situ* electron microscopy and applications. *Proc. Natl. Acad. Sci. (USA)* **102**, 14503–8. Copyright (2005) National Academy of Sciences USA.

address electrically the devices (Fig. 5(b)). In this case, the sensing integrated circuit (IC) chip (MS3110) employed in the capacitance measurement is located outside of the TEM.

Measuring capacitance changes with sub-femtofarad (sub-fF) resolution, as required in this application, is quite challenging. Fortunately, a circuit measuring charge sensing that can mitigate the effect of parasitic capacitance has been developed by the MEMS

community (Senturia 2002). A commercially available IC based on this method, Universal Capacitive Readout MS3110 (Microsensors, Costa Mesa, CA), is employed here. The MEMS device chip is positioned very close to the sensing IC chip (MS3110) in order to minimize the stray capacitance and electromagnetic interference (Fig. 6(a)). The output voltage is proportional to the capacitance change.

Calibration of the displacement–capacitance change relation for the load sensor is critical for this material testing system. To accomplish this endeavor, a particular feature in the movable shuttle is selected as reference in the SEM image. The device is actuated ON and OFF sequentially four times during the SEM scan. The feature corresponding to the ON–OFF actuation cycles is captured in the SEM image
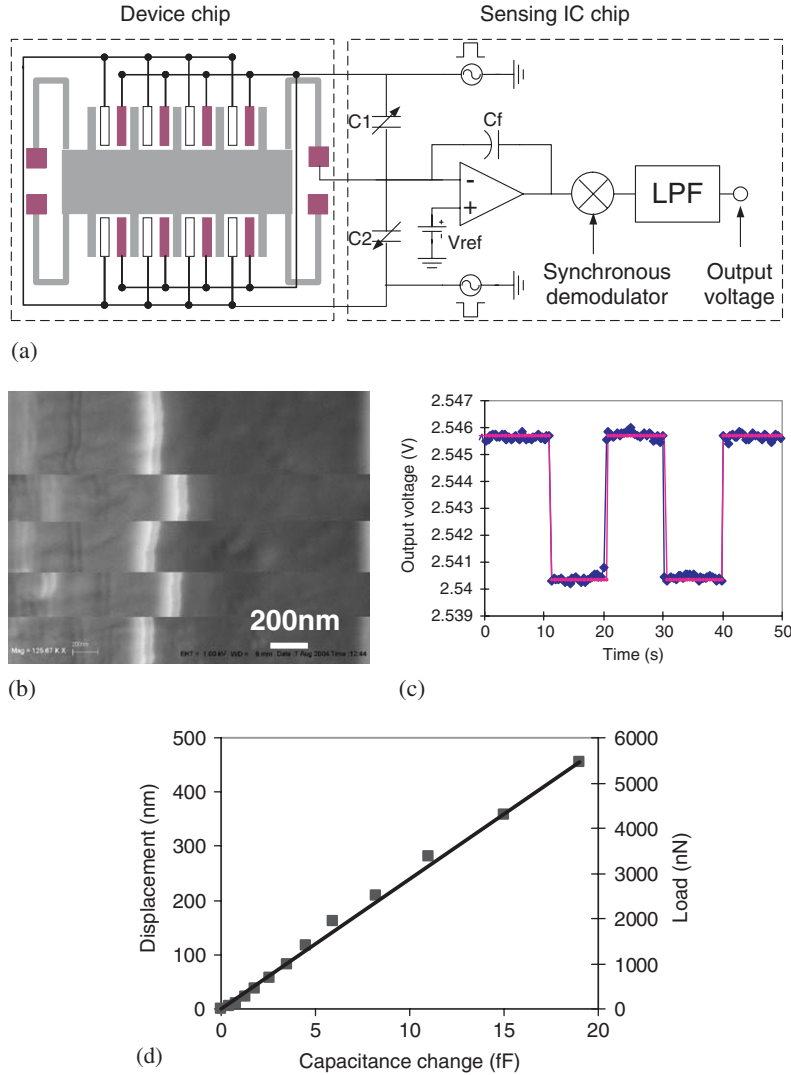

(a)

(b)

(c)

(d)

Figure 6
(a) Schematic of the double chip scheme (device chip and sensing IC chip) used to measure the capacitance change. (b)–(d) Calibration of the load sensor showing the relationship between capacitance change and measured displacement from SEM images at a series of actuation voltages. (b) and (c) Signatures when actuator is at 5 V; (b) reference feature in the SEM image showing a motion of 165 nm due to four ON–OFF actuations, and (c) plot corresponding to a 5.6 fF capacitance change resulting from the same actuation. Both raw data and fitted data are shown in the plot of capacitance measurements. (d) Plot of displacement vs. capacitance change resulting from the calibration.

(Fig. 6(b)), and simultaneously the capacitance change is recorded (Fig. 6(c)). Fig. 6(d) correlates the displacement (load) and the capacitance change. It follows a linear relationship, which agrees well with Eqn. (2). The resolution of the measured capacitance change is 0.05 fF (standard deviation), and the corresponding displacement resolution is 1 nm. For a load sensor with stiffness of 11.8 N m^{-1}, designed for testing carbon nanotubes and nanowires, the load resolution is 12 nN which is quite adequate (Yu *et al.* 2000). Depending on the application, the load resolution can be increased to ∼1 nN by decreasing the sensor stiffness. Additional details on the load sensor calibration can be found in Zhu *et al.* (2005b).

5. Applications

The testing system shown in Fig. 4(a) was employed to test two types of structures: freestanding poly-Si films inside an SEM and CNTs inside a TEM.

For the testing of freestanding thin films, poly-Si was selected because of its well-characterized Young's modulus and failure strength (Sharpe *et al.* 2001), and ease of co-fabrication with the device. Since the minimum feature size by standard photolithography is ∼2 μm, the co-fabricated poly-Si specimen was further nanomachined by focused ion beam (FIB) to reduce the sample minimum dimension to 350–450 nm. A dog-bone-shaped poly-Si specimen with a trapezoidal cross-section was obtained (Fig. 7(a)). Two platinum (Pt) lines (with a spacing of 2.5 μm) were deposited by EBID (Yu *et al.* 2000) in a dual beam FIB/SEM instrument (FEI, Hillsboro, Oregon) for deformation measurement (Fig. 7(b)). Quantification of length increase between these two marks was done by means of image analysis with edge detection software. Two specimens were tested resulting in the stress–strain curves shown in Fig. 7(c). The specimens exhibit nearly the same Young's modulus of 155 GPa ± 5 GPa and failure strengths of 0.7 GPa and 1.42 GPa. The results are consistent with the values reported for MUMPs poly-Si thin films (Sharpe *et al.* 2001). The variation in measured failure strength is to be expected in view of the weakest link theory (Weibull statistics) applicable to brittle materials. Examination of the failure surface, Fig. 7(d), reveals a mirror region at the top right corner of the fracture surface, which is typical of brittle fracture initiation.

MWCNTs were tested *in situ* the TEM (200 keV beam). They were placed on top of the MEMS device following a nanomanipulation procedure described in Zhu and Espinosa (2005). A particular MWCNT was tested inside a TEM using the holder shown in Fig. 5(b). Its outer diameter was ∼130 nm and inner diameter was 99 nm, as shown in Fig. 8(a). The length between the two welding locations was 2.57 μm ± 0.2 μm. The specimen was progressively loaded and its deformation continuously monitored. A fracture

(a) 1 μm

(b) Displacement markers

(c)
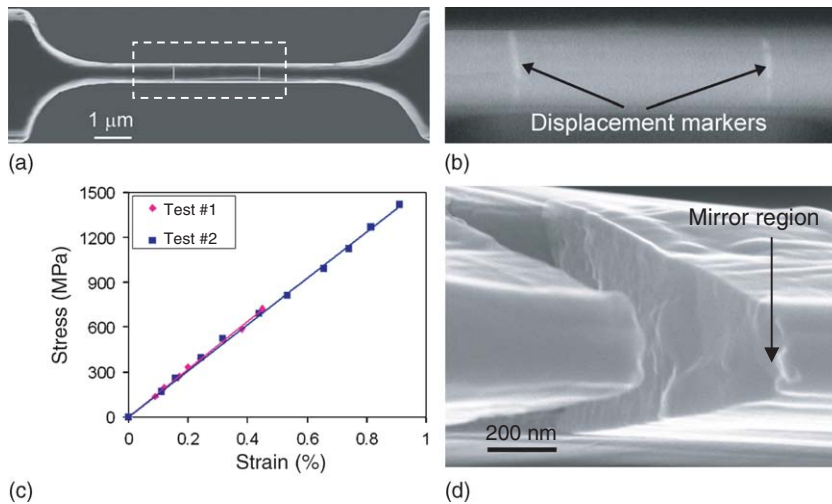
(d) Mirror region — 200 nm

Figure 7
Quantitative *in situ* SEM test of a freestanding polysilicon film. (a) Dog-bone-shaped tensile test specimen. (b) Magnified view of two Pt displacement markers deposited by EBID. (c) Stress–strain curves of two *in situ* SEM tests. Both specimens were 6 μm long and 1.6 μm thick. One had a top width of 0.34 μm and bottom width of 0.87 μm, while the other had a top width of 0.42 μm and bottom width of 1.04 μm. (d) Fracture surface of polysilicon beam showing a mirror region indicative of brittle fracture initiation. Reproduced from Zhu Y, Espinosa H D (2005) An electromechanical material testing system for *in situ* electron microscopy and applications. *Proc. Natl. Acad. Sci. (USA)* **102**, 14503–8. Copyright (2005) National Academy of Sciences, USA.
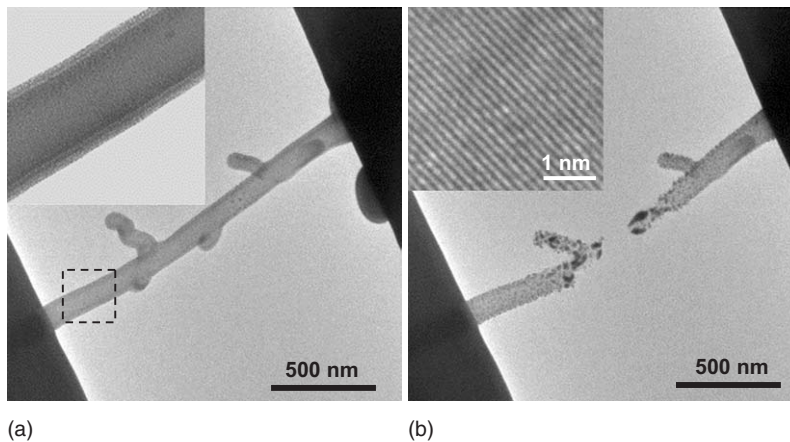
Figure 8

In situ TEM tensile test of an MWCNT. (a) TEM image before the test, (b) TEM image after the test. The inset in (a) shows the multiple graphite shells. The MWCNT has outer diameter of 130 nm and inner diameter of 99 nm. Post failure crystallization can be apparently seen in (b). The inset in (b) is an HRTEM image of a particular nanograin at the fracture region showing that the grain is single crystalline. The three tiny tubes attached to the main tube were present when the MWCNT specimen was taken out from a bundle during nanomanipulation. Reproduced from Zhu Y, Espinosa H D (2005) An electromechanical material testing system for *in situ* electron microscopy and applications. *Proc. Natl. Acad. Sci. (USA)* **102**, 14503–8. Copyright (2005) National Academy of Sciences, USA.

strength of 15.84 GPa and a failure strain of 1.56% was measured. These results are in agreement with those previously reported in Yu *et al.* (2000). However, a new phenomenon was observed during the *in situ* experiment. After failure, the graphite shells disappeared. Instead, a large number of nanoparticles (with diameters ranging from 5 nm to 50 nm) embedded in an amorphous matrix were observed (see Fig. 8(b)). Both high-resolution TEM (HRTEM) and nanodiffraction confirmed that the nanoparticles are single crystals. Both stress and temperature, due to electron beam irradiation and thermal actuation, existed in our experiment. It is possible that the CNTs (graphite sheets) transformed to other phases under this combined loading condition.

Bibliography

Bachtold A, Hadley P, Nakanishi T, Dekker C 2001 Logic circuits with carbon nanotube transistors. *Science* **294**, 1317–20

Chu L L, Que L, Gianchandani Y B 2002 Measurements of material properties using differential capacitive strain sensors. *J. Microelectromech. Syst.* **11**, 489–98

Cui Y, Lieber C M 2001 Functional nanoscale electronic devices assembled using silicon nanowire building blocks. *Science* **291**, 851

Cui Y, Wei Q, Park H, Lieber C M 2001 Nanowire nanosensors for highly sensitive and selective detection of biological and chemical species. *Science* **293**, 1289

Duan X, Huang Y, Agarwal R, Lieber C M 2003 Single-nanowire electrically driven lasers. *Nature (London)* **421**, 241–5

Fennimore A M, Yuzvlnsky T D, Han W Q, Fuhrer M S, Cummings J, Zettl A 2003 Rotational actuators based on carbon nanotubes. *Nature (London)* **424**, 408–10

Fischer E E, Labossiere P E 2002 MEMS fatigue testing to study nanoscale material response. In: *Proc. of the SEM Ann. Conf. on Exp. and Appl. Mech.*, Milwaukee, WI, USA, Sept 25, 2005

Haque M A, Saif M T A 2002 Application of MEMS force sensors for *in-situ* mechanical characterization of nano-scale thin films in SEM and TEM. *Sens. Actuators A* **97–8**, 239–45

Haque M A, Saif M T A 2004 Deformation mechanisms in free-standing nanoscale thin films: a quantitative *in situ* transmission electron microscope study. *Proc. Natl. Acad. Sci. (USA)* **101**, 6335–40

Huang Y, Duan X, Cui Y, Lauhon L J, Kim K-H, Lieber C M 2001 Logic gates and computation from assembled nanowire building blocks. *Science* **294**, 1313–7

Iijima S 1991 Helical microtubules of graphitic carbon. *Nature (London)* **354**, 56

Kahn H, Tayebi N, Ballarini B, Mullen R L, Heuer A H 2000 Fracture toughness of polysilicon MEMS devices. *Sens. Actuators A* **82**, 274–80

Kahn H, Ballarini B, Heuer A H 2001 On-chip testing of mechanical properties of MEMS devices. *MRS Bull.* **26**, 300–1

Kim P, Lieber C M 1999 Nanotube nanotweezers. *Science* **286**, 2148–50

Kong J, Franklin N R, Zhou C, Chapline M G, Peng S, Cho K, Dai H 2000 Nanotube molecular wires as chemical sensors. *Science* **287**, 622–5

Law M, Sirbuly D J, Johnson J C, Goldberger J, Saykally R J, Yang P 2004 Nanoribbon waveguides for subwavelength photonics integration. *Science* **305**, 1269–73

Li L S, Alivisatos A P 2003 Semiconductor nanorod liquid crystals and their assembly on a substrate. *Adv. Mater.* **15**, 408

Pan Z W, Xie S S, Lu L, Chang B H, Sun L F, Zhou W Y, Wang G, Zhang D L 1999 Tensile tests of ropes of very long aligned multiwall carbon nanotubes. *Appl. Phys. Lett.* **74**, 3152–4

Pan Z W, Dai Z R, Wang Z L 2001 Nanobelts of semiconducting oxides. *Science* **291**, 1947

Poncharal P, Wang Z L, Ugarte D, de Heer W A 1999 Electrostatic deflections and electromechanical resonances of carbon nanotubes. *Science* **283**, 1513–6

Salvetat J P, Briggs G A D, Bonard J M, Bacsa R R, Kulik A J, Stockli T, Burnham N A, Forro L 1999 Elastic and shear moduli of single-walled carbon nanotube ropes. *Phys. Rev. Lett.* **82**, 944–7

Senturia S D 2002 *Microsystem Design*. Kluwer Academic Publishers, Boston

Sharpe W N, Jr., Jackson K M, Hemker K J, Xie Z 2001 Effect of specimen size on Young's modulus and fracture strength of polysilicon. *J. Microelectromech. Syst.* **10**, 317–26

Tang W C, Nguyen T-C, Judy M W, Howe R T 1990 Electrostatic-comb drive of lateral polysilicon resonators. *Sens. Actuators A* **21**, 328–31

Treacy M M J, Ebbesen T W, Gibson J M 1996 Exceptionally high Young's modulus observed for individual carbon nanotubes. *Nature (London)* **381**, 678–80

van Arsdell W W, Brown S B 1999 Subcritical crack growth in silicon MEMS. *J. Microelectromech. Syst.* **8**, 319–27

Walters D A, Ericson L M, Casavant M J, Liu J, Colbert D T, Smith K A, Smalley R E 1999 Elastic strain of freely suspended single-wall carbon nanotube ropes. *Appl. Phys. Lett.* **74**, 3803–5

Wang J, Li Y 2003 Rational synthesis of metal nanotubes and nanowires from lamellar structures. *Adv. Mater.* **15**, 445

Wildoer J W G, Venema L C, Rinzler A G, Smalley R E, Dekker C 1998 Electronic structure of atomically resolved carbon nanotubes. *Nature (London)* **391**, 59–62

Wong E W, Sheehan P E, Lieber C M 1997 Nanobeam mechanics: elasticity, strength, and toughness of nanorods and nanotubes. *Science* **277**, 1971–5

Yu M F, Lourie O, Dyer M J, Moloni K, Kelly T F, Ruoff R S 2000 Strength and breaking mechanism of multiwalled carbon nanotubes under tensile load. *Science* **287**, 637–40

Zhu Y, Espinosa H D 2005 An electromechanical material testing system for *in situ* electron microscopy and applications. *Proc. Natl. Acad. Sci. (USA)* **102**, 14503–8

Zhu Y, Corigliano A, Espinosa H D 2005a *Sens. Actuators A* (submitted)

Zhu Y, Moldovan N, Espinosa H D 2005b A microelectromechanical load sensor for *in situ* electron and X-ray microscopy tensile testing of nanostructures. *Appl. Phys. Lett.* **86**, 013506

H. D. Espinosa, Y. Zhu, and N. Moldovan